Interlayer Self-Diffusion and Structure of Chiral Smectic Phases Studied by ^{2}H NMR Exchange Experiment

Jiadi Xu[†] and Ronald Y. Dong*[,†,‡]

Department of Physics and Astronomy, University of Manitoba, Winnipeg, MB, Canada R3T 2N2, and Department of Physics and Astronomy, Brandon University, Brandon, MB, Canada R7A 6A9

Received: October 13, 2005; In Final Form: November 30, 2005

A deuterium two-dimensional exchange NMR technique is used to study the chiral smectic C (Sm*C**) and chiral subphases (SmC^*_{Fi1}, SmC^*_{Fi2}) of a smectogen (*s*)-1-methylheptyl 4′-(4-*n*-decyloxy-benzoyloxy)-biphenyl-4-carboxylate (10B1M7). The aim is to demonstrate how this technique can be combined with sample rotation in the magnetic field to obtain the fast translational self-diffusion constant along the helical pitch in the Sm*C** phase and to shed light on the structure of helicoidal superlattice in the three-layer SmC^*_{Fi1} and four-layer SmC^*_{Fi2} phases. The cross-peak intensities in the 2D exchange spectrum are sensitive to the disposition of molecules in the three- and four-layer base unit. The results support the "asymmetric Clock model" as an appropriate description of the ferrielectric phases in this compound.

1. Introduction

Since the discovery of synclinic ordering in ferroelectric chiral smectic C phase (Sm*C**) of chiral liquid crystals (LC) in 1975,[1] some other chiral tilted smectic phases such as SmC^*_{Fi2} (or SmC^*_{AF}), SmC^*_{Fi1} (or SmC^*_{γ}), and SmC^*_A, which show instead anticlinic ordering,[2−4] have subsequently been found. Significant experimental and theoretical efforts have been directed to investigate the structure and dynamics of these chiral LC materials.[5−9] It is now widely accepted that a typical phase sequence for these chiral materials is SmC^*_α−Sm*C**−SmC^*_{Fi2}−SmC^*_{Fi1}−SmC^*_A upon decreasing temperature and is a result of the relevant interlayer interactions.[9,10] Note that certain phases may not exist in some materials. Although a variety of experimental probes has been used to obtain information on the molecular packing in these phases, including resonant X-ray,[9,11,12] optical rotatory power,[10,13,14] ellipsometry,[15] and dynamic light scattering,[16] only the structures of Sm*C** and SmC^*_A are well documented. Other chiral subphases are still of much current interest. The X-ray scattering experiment gave the first direct structural evidence for distinct superlattice periodicities consisting of two layers in the SmC^*_A phase, three layers in the SmC^*_{Fi1} phase, and four layers in the SmC^*_{Fi2} phase,[9] while the Sm C^*_α phase is a short-pitch version of the Sm*C** phase.[17,18] The exact disposition of molecules is still not clear within the base unit of the SmC^*_{Fi1} and SmC^*_{Fi2} phases. Both symmetry consideration and thermodynamic argument lead to the only possible disposition in the anticlinic phases (φ is a measure of the difference between the azimuthal angles for molecules in the two neighboring layers) shown in Figure 1a.[3,11,17] $\varphi = 0°$ corresponds to the "Ising model",[19] while $\varphi = 120°$ (SmC^*_{Fi1}) or $\varphi = 90°$ (SmC^*_{Fi2}) gives the "Clock model".[20]

Rotational diffusion of molecules has been studied in chiral phases by using the deuteron spin relaxation method,[5,21] while translational diffusion of molecules is harder to observe because of the very low diffusion constant in these phases, especially in anticlinic phases, about 10^{-13} to 10^{-14} m^2/s.[7,22] The angular-dependent ^{2}H NMR can give precise self-diffusion constants in anticlinic phases by making use of intrinsic spatial modulations of the local electric field gradient (EFG). This was demonstrated by a study of the structure and self-diffusion in the SmC^*_A phase.[7] Recently, it has also been extended to ferrielectric phases.[23] Not only the interlayer diffusion was measured, but the molecular arrangements in the ferriphases were also obtained. It was confirmed that the "asymmetric clock model"[24] was appropriate for the ferriphases of 10B1M7. This technique, however, failed in the synclinic Sm*C** phase because of the small variation in the tilt orientation between two neighboring layers. A 2D exchange experiment has been proven to be a powerful method to study slow motions and to determine the structure of polymer and liquid crystals.[25−27] On the basis of the molecular self-diffusion, the relative orientation of molecules has been obtained in powder polymers by ^{13}C 2D exchange experiments.[28,29] In the present study, a ^{2}H 2D exchange experiment is performed on an aligned 10B1M7 sample in the chiral Sm*C** phase to directly observe the interlayer self-diffusion of molecules. To measure the self-diffusion in this phase, the aligned sample must be oriented such that the pitch axis is at an angle with respect to the external magnetic field. In addition, the molecular disposition in the base

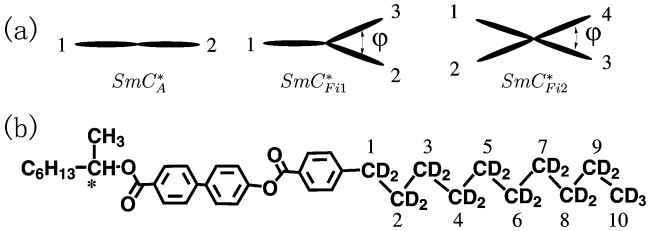

Figure 1. (a) Top view of the disposition of molecules in one base unit of SmC^*_A, SmC^*_{Fi1}, and SmC^*_{Fi2} phases, respectively. The number labels the layer. (b) Molecular structure of a partially deuterated 10B1M7 showing deuteron site labels. The asterisk indicates the chiral carbon center.

* Corresponding author. E-mail: dong@brandonu.ca.
† Department of Physics and Astronomy, University of Manitoba.
‡ Department of Physics and Astronomy, Brandon University.

10.1021/jp055868w CCC: $33.50
Published on Web 01/05/2006

unit is also studied in the anticlinic phases. The results of this study are reported here.

2. Experimental Section

The optically pure 10B1M7[30] is that used in our previous studies[21,23,31] and shows various mesophases at different ranges of temperature. The synthesis and its characterization were reported elsewhere.[30,32] Figure 1b shows the structure of a chain-deuterated 10B1M7 molecule. Its phase sequence and transition temperatures are listed below

$$\text{Iso} \xleftrightarrow{397.5\ \text{K}} \text{Sm}A \xleftrightarrow{378.4\ \text{K}} \text{Sm}C^* \xleftrightarrow{342\ \text{K}} \text{Sm}C^*_{\text{Fi2}} \xleftrightarrow{335\ \text{K}} \text{Sm}C^*_{\text{Fi1}} \xleftrightarrow{330.3\ \text{K}} \text{Sm}C^*_{\text{A}} \xrightarrow{312.1\ \text{K}} \text{Sm}J^*$$

Here, the phase transition temperatures (Iso → Sm*A*, Sm*A* → Sm*C**, and $\text{Sm}C^*_{\text{A}}$ → $\text{Sm}C^*_J$) are determined by the quadrupolar splittings of DNMR spectra[32], while the transition temperatures (Sm*C** → $\text{Sm}C^*_{\text{Fi2}}$, $\text{Sm}C^*_{\text{Fi2}}$ → $\text{Sm}C^*_{\text{Fi1}}$, and $\text{Sm}C^*_{\text{Fi1}}$ → $\text{Sm}C^*_{\text{A}}$) are determined by the angular-dependent DNMR line shapes.[23,33] Notice that these transition temperatures are slightly different from those obtained by the optical method.[30] This is probably due to the deuteration and sample purity. The sample was aligned with the pitch axis along the magnetic field by cooling slowly to the desired temperature in the chiral smectic phases after heating to the clearing temperature. Two-dimensional deuterium exchange spectra were collected on a Bruker Avance 400 solid-state system equipped with a Bruker high-precision goniometer probe. Before collecting the 2D exchange spectrum, the aligned sample was first rotated by 25 degrees with respect to the magnetic field (9.4 T). The field-induced sample realignment was found to be negligible by reproducing the 1D deuterium spectrum after collecting each 2D exchange spectrum. Our experiments show that the sample orientation is very stable up to 90° in the anticlinic phases. In the Sm*C** phase, no orientational flow was observed at rotation angles <60°. The difference is due to the fact that the anticlinic order is far less sensitive to the external magnetic field than the synclinic ordering.[7] A five-pulse sequence $90°-\tau-90°-\tau-t_1-54.7°-t_{\text{mix}}-54.7°-\tau-90°-\tau$ has been used to generate a "cosine" and "sine" exchange spectrum,[34] where $\tau = 20\ \mu$s is the delay for the two 90° refocusing pulses, the exchange mixing time t_{mix} is chosen according to the interlayer self-diffusion constant, and t_1 gives the time increment of the F1 dimension. About 1−5 ms was used for t_{mix} in anticlinic phases, while 10−50 ms was used in the Sm*C** phase. A minimum phase cycle, suggested in ref 34, was used by incrementing all phases through 90°, 180°, and 270° to suppress quadrature images (CYCLOPS). By changing the phases of the two 54.7° pulses,[34] the "cosine" and "sine" spectrum were created by using the same pulse sequence. The pure absorption mode spectrum was obtained by adding the "cosine" and "sine" spectrum. The small effect due to a slight difference between $T_{1\text{Z}}$ and $T_{1\text{Q}}$ was accounted for by multiplying an adjustable factor to either the "sine" or "cosine" spectrum before adding the two spectra. The length of 90° pulse was about 2.8 μs. Recycle delay was about 1 s. With a typical number of 64 t_1 increments, about 1 h was required to collect a 2D exchange spectrum.

3. Theory

A deuterium 2D exchange experiment can give information on the molecular orientation due to the orientational dependence of quadrupolar interaction of spin-1 nuclei on a given molecular unit in the external magnetic field. When neglecting the asymmetry parameter, the NMR frequency is given by

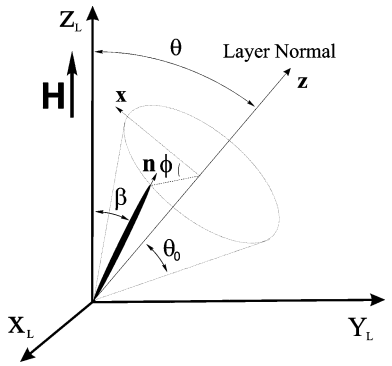

Figure 2. Geometry of a sample rotation experiment. The molecular director is denoted by **n**, which is along the Z_{M} axis of a molecular (X_{M},Y_{M},Z_{M}) frame. (X_{L},Y_{L},Z_{L}) is the laboratory frame, whereas (x,y,z) frame is fixed to the LC smectic layers.

$$\nu^{\pm} = \pm\frac{3}{4}\bar{\nu}_{\text{Q}}\left(\frac{3}{2}\cos^2\beta - \frac{1}{2}\right) \tag{1}$$

where $\bar{\nu}_{\text{Q}} = e\bar{Q}\bar{V}_{zz}/h$ is a time-averaged nuclear quadrupolar coupling constant along the long molecule (Z_{M}) axis, and β is the angle between the direction of the magnetic field and the long molecular axis (Figure 2). When the aligned sample (smectic planar normal) in the goniometer probe is rotated by an angle θ with respect to the magnetic field, the β angle (see Figure 2) can be obtained from the geometry to give[35]

$$\cos\beta = \sin\theta\sin\theta_0\cos\phi + \cos\theta\cos\theta_0 \tag{2}$$

where θ_0 is the molecular tilt angle, and ϕ is the molecular azimuthal angle measured with respect to the plane formed by the layer normal and the magnetic field (i.e., x axis in Figure 2). The observed NMR spectrum is the sum of resonant frequencies from molecules in the helical structure that are uniformly distributed on the surface of a cone with an apex angle given by θ_0 (Figure 2).

When molecules diffuse along the pitch axis, their tilt direction (θ_0, ϕ) will change by following the tilt direction in each smectic layer. In the Sm*C** phase, the tilt direction changes the azimuthal angle by a tiny amount between neighboring layers. Modulation of the NMR frequency by a small variation of the molecular tilt direction introduced by molecular self-diffusions is small and hard to observe in a 1D spectrum.[7] The 2D exchange experiment can give a model-independent reorientational process of molecules for slow dynamic situations. Considering that a pitch length usually includes hundreds of smectic layers, it is a good assumption that the azimuthal angle (ϕ) of the molecular tilt is a linear function of diffusion length l along the pitch axis z, viz., the tilt direction will change by $\delta\phi = 2\pi l/P_{\text{t}}$, where P_{t} is the pitch length. The interlayer self-diffusion is a 1D diffusion problem, and the probability $P(\phi_0,\phi,t)$ of finding a molecule at position ϕ and at time t is given by[36]

$$P(\phi_0,\phi,t) = \frac{1}{\sqrt{4\pi Dt}}\, e^{-(\phi-\phi_0)^2/16\pi^2\varsigma t} \tag{3}$$

where $\varsigma = D/P_{\text{t}}^2$ is treated as a fitting parameter here, and D is a translational diffusion constant. The 2D exchange spectrum $S(f_1, f_2; \phi_0)$ is obtained from summing the "cosine" (cc) and "sine" (ss) spectra, which are the Fourier transform of

the FID given by the following integrals

$$\mathrm{FID0}_{cc}(t_1,t_2;\phi_0,t_{mix}) = \int\int P(\phi_0,\phi,t_{mix}) \cos[2\pi\nu(\phi)t_2] \cos[2\pi\nu(\phi_0)t_1]\, e^{-\sigma^2(t_1^2+t_2^2)/2}\, d\phi\, d\phi_0$$

$$\mathrm{FID0}_{ss}(t_1,t_2;\phi_0,t_{mix}) = \int\int P(\phi_0,\phi,t_{mix}) \sin[2\pi\nu(\phi)t_2] \sin[2\pi\nu(\phi_0)t_1]\, e^{-\sigma^2(t_1^2+t_2^2)/2}\, d\phi\, d\phi_0 \quad (4)$$

where $\exp[-\sigma^2(t_1^2 + t_2^2)/2]$ is to account for the spectral line broadening with σ being a fitting parameter, and $\nu(\phi)$ is given by eqs 1−2. It is important to realize that the slice of this 2D spectrum with $f_1 = \nu(\phi_0)$ is given by the Fourier transform of the following FID with respect to t_2

$$\mathrm{FID}(t_2) = \int P(\phi_0,\phi,t_{mix})\{\cos[2\pi\nu(\phi)t_2] + \sin[2\pi\nu(\phi)t_2]\}\, e^{-\sigma^2 t_2^2/2}\, d\phi \quad (5)$$

Now the projection of the 2D spectrum on the f_1/f_2 dimension is identical with the 1D spectrum obtained by an angular-dependent study, and there are four singularities on both dimensions. Their positions are given by[35]

$$s_1^{\pm} = \pm\frac{3}{4}\bar{\nu}_Q\left[1 - \frac{3}{2}\sin^2(\theta - \theta_0)\right]$$

$$s_2^{\pm} = \pm\frac{3}{4}\bar{\nu}_Q\left[1 - \frac{3}{2}\sin^2(\theta + \theta_0)\right] \quad (6)$$

where s_1 and s_2 correspond to $\phi_0 = 180°$ and 0°, respectively. Equation 5 provides a simple way to extract the diffusion constant D by fitting the $f_1 = \nu(\phi_0)$ slice of the 2D exchange spectrum (e.g., $\phi_0 = 180°$ or 0°).

In the anticlinic phases, the tilt direction of two neighboring layers can alternate by a larger angle. Although self-diffusions in these phases are almost 2 orders of magnitude lower than that of the synclinic phase,[22] the dynamic effect can still be observed in angular-dependent 1D spectra, and the diffusion constant can be obtained from the dynamic-modulated line shapes.[23] In an intermediate dynamic situation, i.e., the NMR frequency changes during the evolution and detection period, the 2D exchange spectrum is complicated by the dynamic modulation, but the information on the molecular arrangement can still be obtained. Because of the low diffusion constant, diffusion over a long distance is hard to observe in anticlinic phases. Hence only interlayer jumps are considered as a multisite jump problem, i.e., two-site in the SmC_A^* phase, three-site in the SmC_{Fi1}^* phase, and four-site in the SmC_{Fi2}^* phase.[23] Defining Ω as the probability of the molecule jumping from one layer to one of the two neighboring layers per unit time, and taking the jump between two neighboring sites as a stochastic process, the time signal (FID) in a ^{2}H 2D exchange experiment for a base unit and at a particular azimuthal angle ϕ_0 is obtained from the Bloch−McConnell equation.[25,27,37,38] The FID of the "cosine" spectrum is

$$\mathrm{FID0}_{cc}(t_1,t_2;\phi_0,t_{mix}) = \vec{\mathbf{1}}\cdot Re[e^{(\Pi+\Gamma)t_2}]\, e^{\Pi t_{mix}} Re[e^{(\Pi+\Gamma)t_1}\mathbf{M_0}] \quad (7)$$

and the FID of the "sine" spectrum is

$$\mathrm{FID0}_{ss}(t_1,t_2;\phi_0,t_{mix}) = \vec{\mathbf{1}}\cdot Im[e^{(\Pi+\Gamma)t_2}]\, e^{\Pi t_{mix}} Im[e^{(\Pi+\Gamma)t_1}\mathbf{M_0}] \quad (8)$$

where T_1 relaxation during t_{mix} has been neglected, $\mathbf{M_0}$ is a magnetization vector immediately after the first 90° pulse whose component M_{0j} is the initial jth z magnetization, Π is the kinetic matrix (or exchange matrix) describing the stochastic jump process between neighboring sites,

$$\Pi(SmC_A^*) = \begin{pmatrix} -2\Omega & 2\Omega \\ 2\Omega & -2\Omega \end{pmatrix}$$

$$\Pi(SmC_{Fi1}^*) = \begin{pmatrix} -2\Omega & \Omega & \Omega \\ \Omega & -2\Omega & \Omega \\ \Omega & \Omega & -2\Omega \end{pmatrix}$$

$$\Pi(SmC_{Fi2}^*) = \begin{pmatrix} -2\Omega & \Omega & 0 & \Omega \\ \Omega & -2\Omega & \Omega & 0 \\ 0 & \Omega & -2\Omega & \Omega \\ \Omega & 0 & \Omega & -2\Omega \end{pmatrix} \quad (9)$$

and Γ is a diagonal matrix of the NMR frequencies and is given by

$$\begin{pmatrix} -i\omega(\phi_0) & 0 \\ 0 & -i\omega(\phi_0+\pi) \end{pmatrix}$$

$$\begin{pmatrix} -i\omega(\phi_0+\pi) & 0 & 0 \\ 0 & -i\omega(\phi_0-\varphi/2) & 0 \\ 0 & 0 & -i\omega(\phi_0+\varphi/2) \end{pmatrix}$$

$$\begin{pmatrix} -i\omega(\phi_0-\varphi/2) & 0 & 0 & 0 \\ 0 & -i\omega(\phi_0+\varphi/2) & 0 & 0 \\ 0 & 0 & -i\omega(\phi_0+\pi-\varphi/2) & 0 \\ 0 & 0 & 0 & -i\omega(\phi_0+\pi+\varphi/2) \end{pmatrix} \quad (10)$$

for the SmC_A^*, SmC_{Fi1}^*, and SmC_{Fi2}^*, respectively, where $\omega(\phi_0) = 2\pi\nu(\phi_0)$. For the studied anticlinic phases, all layers are equivalent. Therefore, $\mathbf{M_0} = [1/2, 1/2]^T$ (SmC_A^*), $[1/3, 1/3, 1/3]^T$ (SmC_{Fi1}^*), $[1/4, 1/4, 1/4, 1/4]^T$ (SmC_{Fi2}^*) are taken for convenience. In our study, only the simple case of $t_{mix} \gg \tau_c$ ($\tau_c \approx 1/\Omega$) is considered. The observed "cosine" and "sine" exchange spectrum are a linear superposition of all the tilt directions, and can be obtained by Fourier transform over t_1 and t_2 of the FID calculated from

$$\mathrm{FID}_{cc}(t_1,t_2;t_{mix}) = \int_0^{2\pi} \mathrm{FID0}_c(t_1,t_2;\phi_0,t_{mix})\, d\phi_0 \quad \text{("cosine"FID)}$$

$$\mathrm{FID}_{ss}(t_1,t_2;t_{mix}) = \int_0^{2\pi} \mathrm{FID0}_s(t_1,t_2;\phi_0,t_{mix})\, d\phi_0 \quad \text{("sine"FID)} \quad (11)$$

By comparing the simulated 2D exchange spectrum with the experimental spectrum, the molecular arrangement can be obtained in the anticlinic phases.

4. Results and Discussion

4.1. Smectic-C* Phase Study. Several 2D exchange spectra were collected at 344.8 K in SmC* phase with different mixing times. Our experiment shows that the cross-peaks are hard to observe for $t_{mix} < 5$ ms, and there is no significant change in the 2D exchange spectrum when $t_{mix} > 20$ ms, indicating that

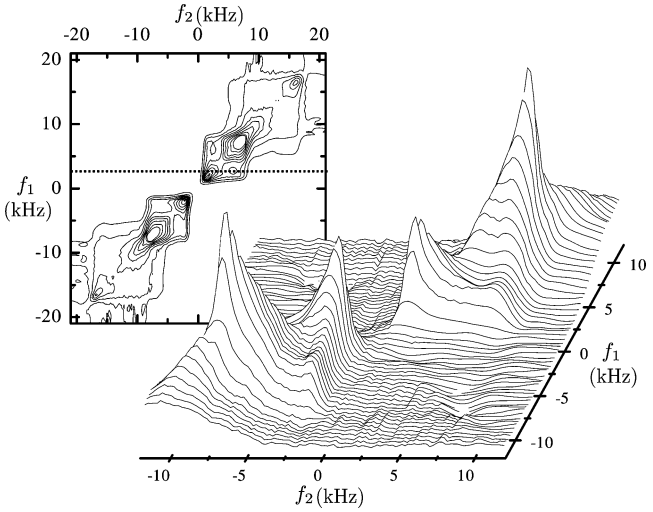

Figure 3. Two-dimensional ^{2}H exchange experiment collected at 344.8 K in Sm*C** phase with a rotation angle $\theta = 25°$ and $t_{mix} = 10$ ms. The spectrum was symmetrized with respect to the diagonal axis. Only the methyl group (C_{10} ^{2}H) is emphasized in the surface plot for clarity. Contour plot gives the C_{10} and C_9 ^{2}H peaks. Dashed line is the slice that is shown in Figure 5.

20 ms is already much larger than τ_c. Therefore, the spectrum collected with a mixing time t_{mix} between 5 and 10 ms is best for extracting the self-diffusion constant. Figures 3 and 4 show the 2D spectrum collected with $t_{mix} = 10$ and 50 ms, respectively, while other experimental parameters are identical for these two spectra. Because of the serious overlaps among the ^{2}H peaks, only ^{2}H peaks of C_{10} and C_9 are plotted. From the singularity peaks $s_1^{\pm}$, $s_2^{\pm}$, $\bar{\nu}_Q = 10.6 \pm 0.3$ kHz and $\theta_0 = 19 \pm 2°$ were calculated by using eq 6 at 344.8 K. The 2D exchange spectrum is harder to fit, especially because of the spectral overlap from neighboring deuterons; instead the 1D spectrum from the slice $f_1 = s_1$ (or $f_1 = \nu(\pi)$), which is indicated by a dashed line in Figures 3−4, was fitted for several mixing times with four parameters θ_0, $\bar{\nu}_Q$, σ, and ς (eq 5), to obtain the diffusion constant. Typical line shapes of 1D slices and their simulations are shown in Figure 5. The positions of the two singularities determine θ_0, $\bar{\nu}_Q$, while the relative intensities of the two singularities are controlled by ςt_{mix}, which appears in eq 3. The θ_0, $\bar{\nu}_Q$ obtained from the fitting is consistent with the values obtained above within the experimental error. The simulated 2D exchange spectrum was then constructed by using the derived fitting parameters, which are listed in Table 1. A ς value of (4.5 ± 0.3) s^{-1} was obtained from the fitting, from which the diffusion constant can be obtained because $D = \varsigma P_t^2$. The pitch length P_t is, however, unknown for 10B1M7, but the layer thickness has been measured as a function of temperature in this compound (3.52 nm at this temperature).[22] An estimated value $P_t = 1.06$ μm is obtained by supposing that one pitch length includes 300 smectic layers. Then, the diffusion constant is $D \approx 5.1 \times 10^{-12}$ m^2/s at 344.8 K. Note the value is about a factor of 3 lower than the reported value 1.7×10^{-11} m^2/s.[22] The discrepancy is likely due to the uncertainty in the number of layers in one pitch length. The reconstructed 2D exchange spectra for $t_{mix} = 10$ and 50 ms are shown in Figures 6 and 7, respectively. They are in good agreement with the observed 2D spectra.

TABLE 1: Fitting Parameters for the Three Typical Temperatures

temp (K)	θ_0 (deg)	$\bar{\nu}_Q$ (kHz)	σ (kHz)	D ($\times 10^{-14}$ m^2/s)	φ
344.8 (Sm*C**)	21 ± 2	10.5 ± 0.3	1 ± 0.2	510	
338.3 (SmC^*_{Fi2})	21 ± 2	11 ± 0.3	3 ± 0.3	1.2	25 ± 5
332.2 (SmC^*_{Fi1})	22 ± 2	12.3 ± 0.3	3.5 ± 0.3	2.5	20 ± 5

4.2. Anticlinic Smectic-*C Phases Study.** Figure 8 shows the 2D exchange spectrum collected in the SmC^*_A phase at 320.5 K with $t_{mix} = 4$ ms. The simulated exchange spectrum of SmC^*_A phase at the sample rotation angle $\theta = 25°$ is shown in Figure 9. The four singularities $s_1^{\pm}$, $s_2^{\pm}$ are same as those in Sm*C** phase (eq 6), and a strong center peak appears because of the interlayer jump. The cross-peak positions in the 2D exchange spectrum are given by $f_1 = \nu(\phi)$, $f_2 = \nu(\phi + \pi)$ ($\phi = 0$ or π). The simulated spectrum is consistent with the observed spectrum (Figure 8). The parameters used for the simulation in Figure 9 are the typical values for this phase. No fitting has been performed. Because the molecular arrangement in SmC^*_A phase is clearly known, attention is therefore placed on the ferrielectric phases. Again, only NMR signals of C_{10} and C_9 peaks are emphasized. The observed exchange spectrum in the SmC^*_{Fi1} phase at 332.2 K is plotted in Figure 10. A strong center peak is evident because of the relatively high interlayer

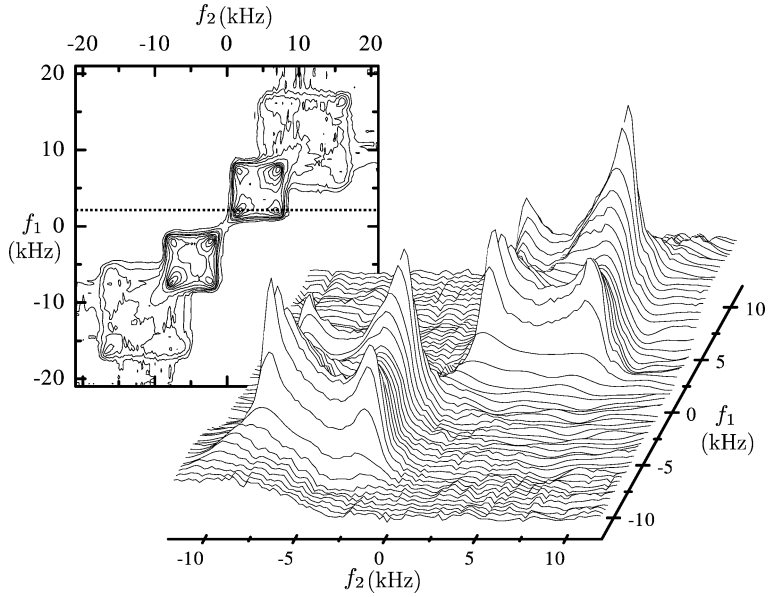

Figure 4. Two-dimensional ^{2}H exchange experiment for $t_{mix} = 50$ ms with the same condition as Figure 4.

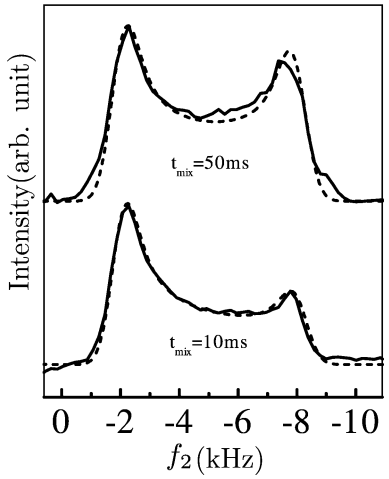

Figure 5. One-dimensional slices (solid lines) taken from the 2D exchange spectrum shown in Figures 3 and 4, together with the simulated spectra (dashed lines) with $\bar{\nu}_Q = 10.9$ kHz and $\theta_0 = 20°$, $\sigma = 2.5$ kHz and $\varsigma = 4.5$ s^{-1}.

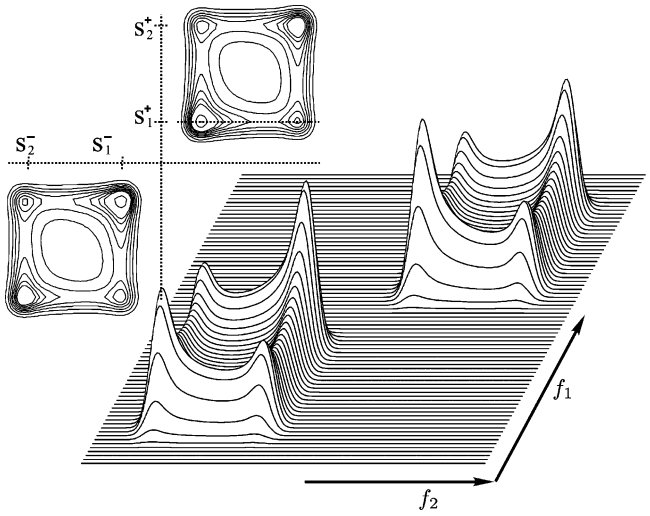

Figure 6. Surface plot of the reconstructed spectrum of Sm*C** phase for the case of $t_{mix} = 10$ ms by using the parameters listed in Figure 5. Top left figure shows the corresponding contour plot. The slice taken from the dashed line gives a 1D fitted spectrum plotted in 5. The four singularities are indicated by using $S_1^{\pm}$, $S_2^{\pm}$.

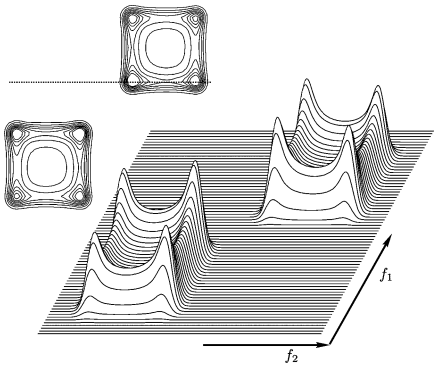

Figure 7. Surface and contour plot of a simulated spectrum of Sm*C** phase for the case of $t_{mix} = 50$ ms. Other parameters are identical with those used in Figure 6.

jump rate, and the intensities of cross-peaks are much smaller than those of the SmC_A^* phase. However, the spectral line shape is still similar to those of the SmC_A^* phase. This means that the φ angle is small. Our simulations plotted in Figure 11 for different φ angles also verify this. For $\varphi < 50°$, the

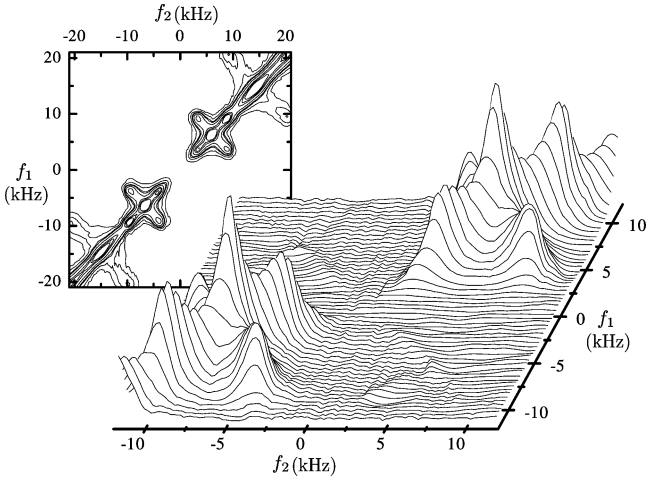

Figure 8. Two-dimensional ^{2}H exchange experiment collected at 320.5 K in SmC_A^* phase with a rotation angle $\theta_0 = 25°$ and $t_{mix} = 4$ ms. Only ^{2}H signal of the methyl (C_{10}) group is emphasized in the surface plot for clarity. The contour plot gives the C_{10} and C_9 ^{2}H peaks.

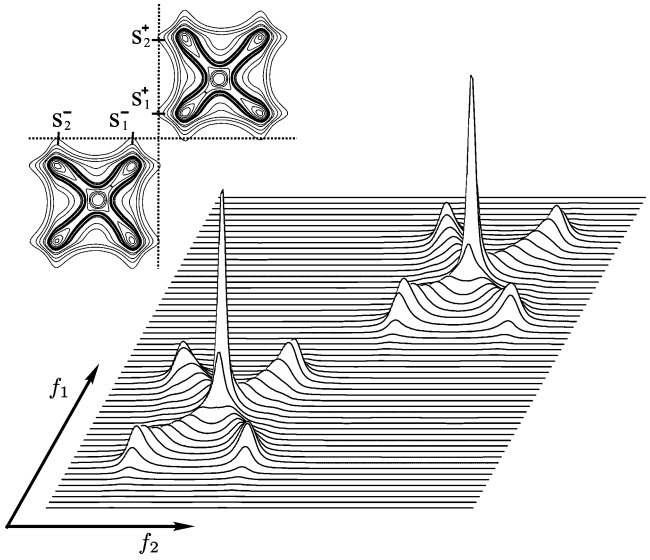

Figure 9. Surface plot of simulated exchange spectrum of SmC_A^* phase at $\theta = 25°$ according to eqs 11 for the case of $t_{mix}/\tau_c \rightarrow \infty$. Top left figure is the corresponding contour plot, and the singularities are indicated by using $S_1^{\pm}$, $S_2^{\pm}$. $\bar{\nu}_Q = 10.5$ kHz, $\theta_0 = 21°$, $\sigma = 1$ kHz, and $\Omega = 1$ kHz.

determination of the φ angle is difficult based on the simulation of the 2D spectrum. Therefore, it is better to extract the φ angle by fitting the 1D slice taken from the 2D exchange spectrum. The two slices, which were used for fitting, are indicated in Figure 10. Although five parameters were used for the fitting, reliable values could still be obtained. The singularity frequencies in slice 1 and 2 gave the values of θ_0 and $\bar{\nu}_Q$, and the line shapes of slice 1 and 2 determined the interlayer jump rate Ω (giving $\Omega = 2.8 \pm 0.3$ kHz) and the φ value, as well as the σ value (3.5 ± 0.3 kHz). These parameters are also summarized in Table 1. However, the overlap of signal from the C_9 deuteron site, which can be seen from the shoulder of the line shape in Figure 12a, and the selection of slice 2 can still cause a relatively large uncertainty in determining φ value, i.e., $\varphi = 20 \pm 5°$.

The same method was also applied to the SmC_{Fi2}^* phase. The 2D exchange spectrum collected at 338.3 K is plotted in Figure 13. The close resemblance of exchange spectra collected in the SmC_{Fi1}^* and SmC_{Fi2}^* phases indicates again a small φ angle.

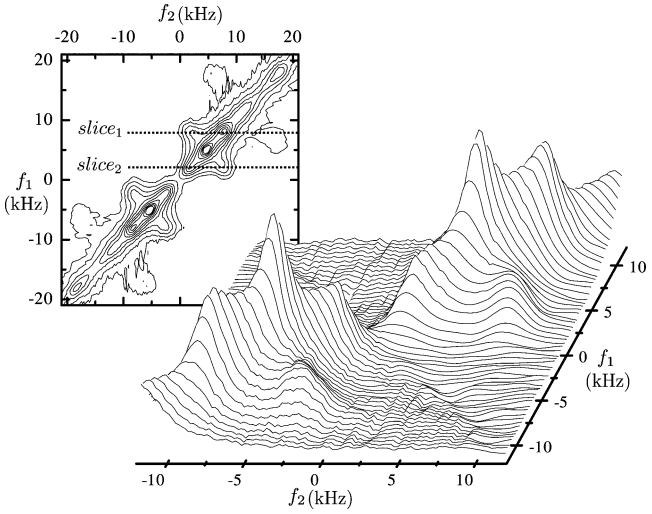

Figure 10. Two-dimensional ^{2}H exchange experiment collected at 332.2 K in SmC^*_{Fi1} phase with $t_{mix} = 2$ ms. Only the methyl group (C_{10} ^{2}H) is emphasized in the surface plot for clarity. The contour plot gives the C_{10} and C_9 ^{2}H peaks.

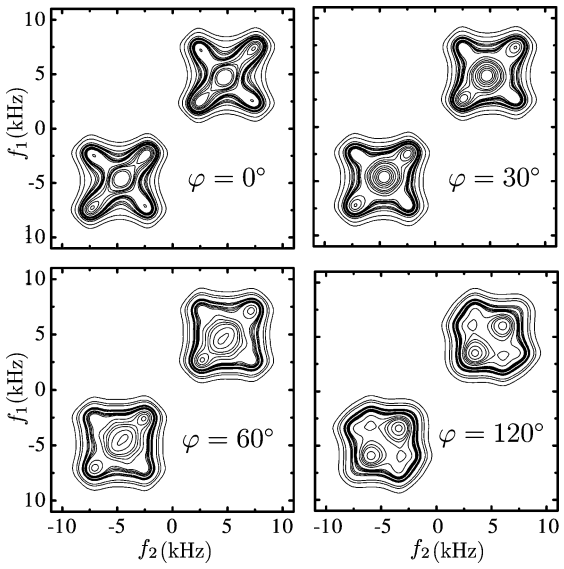

Figure 11. Simulated 2D exchange spectrum of SmC^*_{Fi1} for some typical φ values. $t_{mix} = 2$ ms, σ =2.5 kHz, $\theta_0 = 20°$, and typical interlayer jump rate $\Omega = 2.5$ kHz in this phase are used for simulation.

This is verified by the simulated exchange spectra for different φ angles (Figure 14). The simulation also shows that the line shape of 2D spectrum for $\varphi < 45°$ is not sensitive to the φ angle. The exact φ value was obtained by fitting the 1D spectrum by using the same method employed in the SmC^*_{Fi1} phase. The two slices are taken from the positions indicated by the dashed lines in Figure 13. The fitted 1D spectra and reconstructed 2D exchange spectrum are plotted in Figure 15, giving a φ value of $25 \pm 5°$ and $\Omega = 5.2 \pm 0.4$ kHz. Note that the intensities of slice 1 are much higher than those of slice 2 because of the high interlayer jump value, and the interference of C_9 ^{2}H sites is almost absent (Figure 15a).

From the above analysis, it is clear that the "asymmetric clock model" (or "deformed clock model")[39] is a proper description of the molecular arrangement in the ferrielectric phases. The φ angles found in the ferriphases are also in good agreement with the value determined in MHDDOPTCOB,[11,15] where $\varphi = 18°$ is found. From the interlayer jump Ω, the translational self-discussion constant D can be obtained by $D = 4L^2\Omega/\pi^2$ (L is

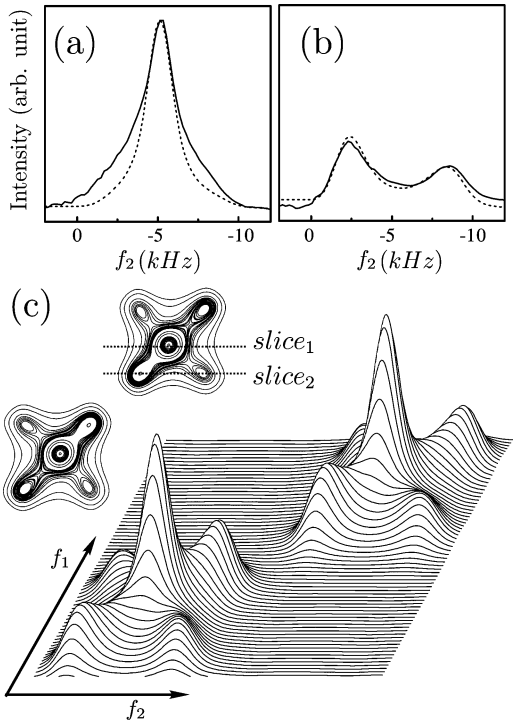

Figure 12. One-dimensional spectrum taken from slice 1 (a) and slice 2 (b) of 2D exchange spectrum in Figure 10 together with their fitted spectra (dotted line), which gives $\theta_0 = 22 \pm 2°$, $\sigma = 3.5 \pm 0.3$ kHz, $\bar{\nu}_Q = 12.3 \pm 0.3$ kHz, $\Omega = 2.8 \pm 0.3$ kHz, and $\varphi = 20 \pm 5°$. The reconstructed 2D exchange spectrum using the parameters obtained above is also plotted (c).

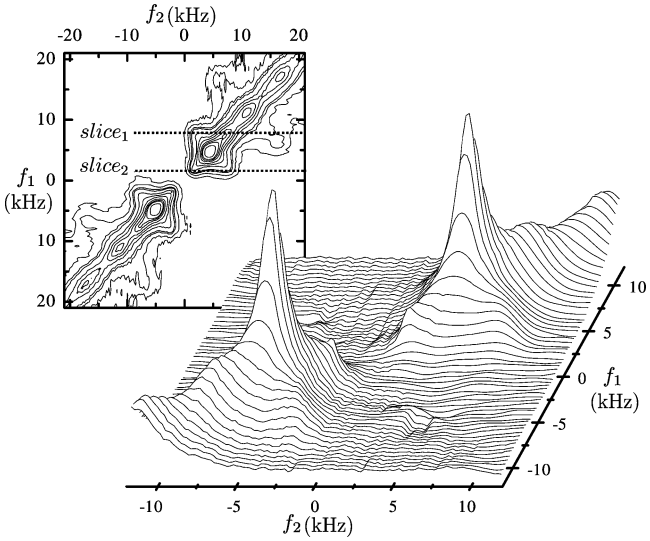

Figure 13. Two-dimensional ^{2}H exchange experiment collected at 338.3 K in SmC^*_{Fi2} phase with $t_{mix} = 1$ ms. Only the methyl group (C_{10} ^{2}H) is emphasized in the surface plot for clarity. The contour plot gives the C_{10} and C_9 ^{2}H peaks.

the layer thickness).[33] Then D (332.2 K) $= 1.2 \times 10^{-14}$ m^2/s and D (338.3 K) $= 2.5 \times 10^{-14}$ m^2/s (Table 1) are based on L = 3.5 nm determined from the X-ray method for the same molecule.[22] These values are about 2 orders of magnitude lower than the diffusion constant of SmC^* phase. The same conclusion was also obtained by the static fringe field NMR diffusometry measurements,[22] although their values in the ferriphase are slightly higher. It is, therefore, useful to apply modern pulse field gradient techniques[40] to measure the self-diffusion constant in the various chiral phases of 10B1M7 for direct comparison with the present results.

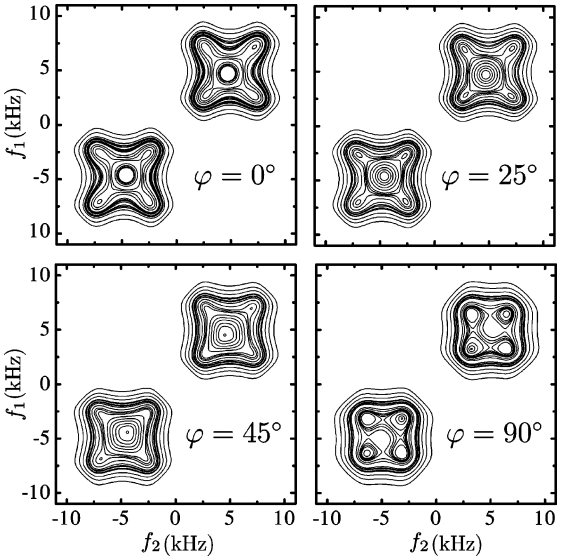

Figure 14. Simulated 2D exchange spectrum of SmC^*_{Fi2} for some typical φ values. $t_{mix} = 1$ ms, $\sigma = 2.5$ kHz, $\theta_0 = 20°$, and $\Omega = 4$ kHz are used for simulation.

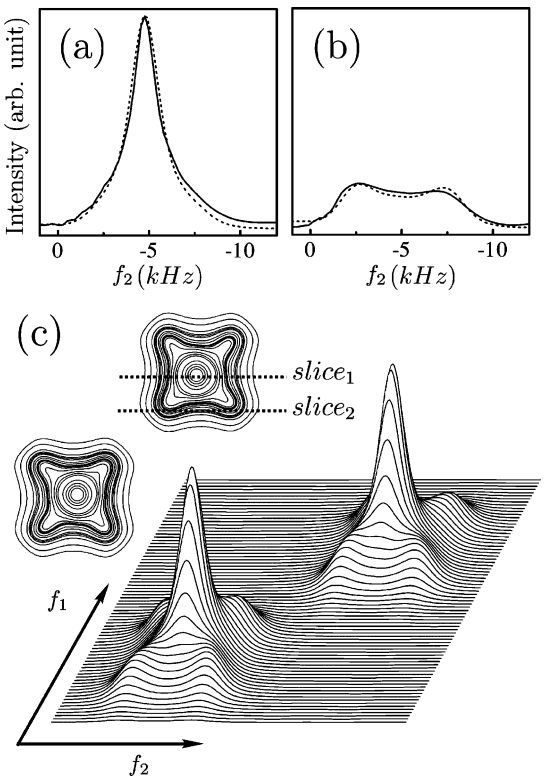

Figure 15. One-dimensional spectrum taken from slice 1 (a) and slice 2 (b) of 2D exchange spectrum in Figure 13 together with their fitted spectra (dotted line), which gives $\theta_0 = 21 \pm 2°$, $\sigma = 3 \pm 0.3$ kHz, $\bar{\nu}_Q = 11 \pm 0.3$ kHz, $\Omega = 5.2 \pm 0.4$ kHz, and $\varphi = 25 \pm 5°$. (c) The reconstructed 2D exchange spectrum using the parameters obtained above is also plotted.

5. Conclusion

Our experiment shows that a 2D exchange experiment can be applied to study the dynamics and structure of chiral smectic C phases. The "pseudopowder" spectra from an aligned sample rotated in the NMR field can be used to extract the translational diffusion constant in the Sm*C** phase. Another benefit of an aligned sample is that it gives access to some jump angles that cannot be distinguished by an exchange experiment on a powder sample. This is due to the fact that an exchange experiment on a powder sample (where θ is random) gives the same line shape for jump angles ϕ and $\pi-\phi$, while jump angles ϕ and $2\pi-\phi$ give the same exchange line shape in an aligned sample. Structural distortions under an external magnetic field may also exist[41] in these phases. However, this can be monitored by the relative intensities between the singularities $s_1^{\pm}$ and $s_2^{\pm}$.[23,33] Our experiment shows that the distortion under the small rotation angle used in this sample can be neglected. Incidentally, it is impossible to produce a "true" powder sample by heating to the chiral smectic phases because the magnetic torque on the molecules could cause partial alignment of the helices. A monodeuterated sample will be useful to avoid interference from other deuterated sites and to simplify the observed 2D exchange spectrum, thereby leading to more accurate φ and Ω values. This method also shows the potential for exploring other phase structures that show large alternation of the molecular tilt direction such as the Sm C^*_α phase.

Acknowledgment. The Natural Sciences and Engineering Council of Canada, Canada Foundation of Innovation, and Brandon University are thanked for their financial support. We thank Prof. C. A. Veracini for the use of the partially deuterated 10B1M7.

References and Notes

(1) Meyer, R. B.; Liebert, L.; Strzelecki, L.; Keller, P. *J. Phys. (Paris)* **1975**, *36*, L69.
(2) Chandani, A. D. L.; Gorecka, E.; Ouchi, Y.; Takezoe, H.; Fukuda, A. *Jpn. J. Appl. Phys.* **1989**, *28*, L1265.
(3) Matsumoto, T.; Fukuda, A.; Johno, M.; Motoyama, Y.; Yui, T.; Seomunc, S.; Yamashitad, M. *J. Mater. Chem.* **1999**, *9*, 2051.
(4) Goodby, J. W.; Slaney, A. J.; Booth, C. J.; Nishiyama, I.; Vuijk, J. D.; Styring, P.; Toyne, K. *J. Mol. Cryst. Liq. Cryst.* **1994**, *243*, 231.
(5) Catalano, D.; Cifelli, M.; Geppi, M.; Veracini, C. *J. Phys. Chem. A* **2001**, *105*, 34.
(6) Galerne, Y.; Liebert, L. *Phys. Rev. Lett.* **1991**, *66*, 2891.
(7) Zalar, B.; Gregorovic, A.; Blinc, R. *Phys. Rev. E* **2000**, *62*, R37.
(8) Dolganov, P. V.; Zhilin, V. M.; Dolganov, V. K. *Phys. Rev. E* **2003**, *67*, 041716.
(9) Mach, P.; Pindak, R.; Levelut, A.-M.; Barois, P.; Nguyen, H. T.; Huang, C. C.; Furenlid, L. *Phys. Rev. Lett.* **1998**, *81*, 1015.
(10) Cepic, M.; Gorecka, E.; Pociecha, D.; Zeks, B.; Nguyen, H. T. *J. Chem. Phys.* **2002**, *117*, 1817.
(11) Cady, A.; Pitney, J. A.; Pindak, R.; Matkin, L. S.; Watson, S. J.; Gleeson, H. F.; Cluzeau, P.; Barois, P.; Levelut, A.-M.; Caliebe, W.; Goodby, J. W.; Hird, M.; Huang, C. C. *Phys. Rev. E* **2001**, *64*, 050702R.
(12) Gorkunov, M.; Pikin, S.; Haase, W. *JETP Lett.* **1999**, *69*, 243.
(13) Akizuki, T.; Miyachi, K.; Takanishi, Y.; Ishikawa, K.; Takezoe, H.; Fukuda, A. *Jpn. J. Appl. Phys.* **1999**, *138*, 4832.
(14) Musevic, I.; Skarabot, M. *Phys. Rev. E* **2003**, *64*, 051706.
(15) Johnson, P. M.; Olson, D. A.; Pankratz, S.; Nguyen, T.; Goodby, J.; Hird, M.; Huang, C. C. *Phys. Rev. Lett.* **2000**, *84*, 4870.
(16) Konovalov, D.; Nguyen, H. T.; Copic, M.; Sprunt, S. *Phys. Rev. E* **2001**, *64*, 010704R.
(17) Dzik, E.; Mieczkowski, J.; Gorecka, E.; Pociecha, D. *J. Mater. Chem.* **2005**, *15*, 1255.
(18) Hirst, L. S.; Watson, S. J.; Gleeson, H. F.; Cluzeau, P.; Barois, P.; Pindak, R.; Pitney, J.; Cady, A.; Johnson, P.; Huang, C.; Levelut, A. M.; Srajer, G.; Pollmann, J.; Caliebe, W.; Seed, A.; Herbert, M. R.; Goodby, J. W.; Hird, M. *Phys. Rev. E* **2002**, *65*, 041705.
(19) Fukuda, A.; Takanishi, Y.; Isozaki, T.; Ishikawa, K.; Takezoe, H. *J. Mater. Chem.* **1994**, *4*, 997.
(20) Cepic, M.; Zeks, B. *Mol. Cryst. Liq. Cryst.* **1995**, *263*, 61.
(21) Dong, R. Y.; Zhang, J.; Veracini, C. A. *Solid State NMR* **2005**, *28*, 173.
(22) Cifelli, M.; Domenici, V.; Veracini, C. A. *Mol. Cryst. Liq. Cryst.* **2005**, *429*, 167.
(23) Xu, J.; Veracini, C. A.; Dong, R. Y. *Phys. Rev. E* **2006**, in press.
(24) Lorman, V. L.; Bulbitch, A. A.; Toledano, P. *Phys. Rev. E* **1994**, *49*, 1367.
(25) Jeener, J.; Meier, B. H.; Bachmann, P.; Ernst, R. R. *J. Chem. Phys.* **1979**, *71*, 4547.
(26) Leisen, J.; Werth, M.; Boeffel, C.; Spiess, H. W. *J. Chem. Phys.* **1979**, *71*, 4547.

(27) Schmidt-Rohr, K.; Spiess, H. W. *Multidimensional Solid-State NMR and Polymers*; Academic Press: New York, 1994.
(28) Tycko, R.; Dabbaagh, G. *J. Am. Chem. Soc.* **1991**, *113*, 3592.
(29) Henrichs, P. M.; Linder, M. *J. Magn. Reson.* **1984**, *58*, 458.
(30) Goodby, J.; Patel, J.; Chin, E. *J. Mater. Chem.* **1992**, *2*, 197.
(31) Dong, R. Y.; Chiezzi, L.; Veracini, C. A. *Phys. Rev. E* **2002**, *65*, 041716.
(32) Catalano, D.; Cavazza, M.; Chiezzi, L.; Geppi, M.; Veracini, C. *Liq. Cryst.* **2000**, *27*, 621.
(33) Xu, J.; Veracini, C. A.; Dong, R. Y. *Phys. Rev. E* **2005**, *72*, 051703.
(34) Schaefer, D.; Leisen, J.; Spiess, H. W. *J. Magn. Reson., Ser. A* **1995**, *115*, 60.
(35) Wu, B. G.; Doane, J. W. *J. Magn. Reson.* **1987**, *75*, 39.
(36) Crank, J. *Mathematics of Diffusion*; Oxford University Press: New York, 1975.
(37) McConnell, H. M. *J. Chem. Phys.* **1958**, *28*, 430.
(38) Abragam, A. *Principles of Nuclear Magnetism*; Oxford University Press: Oxford, 1962.
(39) Lorman, V. L. *Liq. Cryst.* **1996**, *20*, 267.
(40) Dvinskikh, S. V.; Furó, I.; Zimmermann, H.; Maliniak, A. *Phys. Rev. E* **2002**, *65*, 050702R.
(41) Xu, J.; Veracini, C. A.; Dong, R. Y. *Chem. Phys. Lett.* **2005**, *416*, 47.